coatings

MDPI

Article

Amorphous Alumina ALD Coatings for the Protection of Limestone Cultural Heritage Objects

Gillian P. Boyce [1,2], Suveena Sreenilayam [1], Eleonora Balliana [2], Elisabetta Zendri [2] and Raymond J. Phaneuf [1,*]

[1] Department of Materials Science & Engineering, University of Maryland, College Park, MD 20742, USA; gpboyce@umd.edu (G.P.B.); ssreenil@terpmail.umd.edu (S.S.)
[2] Department of Environmental Sciences, Informatics, Statistics, Ca' Foscari University Venice, 30123 Venice, Italy; eleonora.balliana@unive.it (E.B.); elizen@unive.it (E.Z.)
* Correspondence: phaneuf@umd.edu; Tel.: +1-301-405-6566

Abstract: From natural erosion to pollution-accelerated decay, stone cultural heritage deteriorates constantly through interactions with the environment. Common protective treatments such as acrylic polymers are generally prone to degradation and loss of performance, and they are often limited in their ability to achieve uniform and conformal coverage across a stone's topographical features. In this work, atomic layer deposition (ALD) was explored to address these issues by growing protective amorphous alumina coatings on compact carbonate (Istria) stone. ALD protective coatings, unlike coatings produced by traditional methods, do not significantly alter morphology by filling open pores or accumulating on the surface in more compact areas. Our morphological and spectroscopic investigations revealed that the ALD alumina films deposited uniformly over the surfaces of Istria stone, without significantly altering the topography or appearance. The protective effects of the ALD coatings were investigated by aqueous acid immersion. The solution pH, along with the Ca^{2+} concentration, was tracked over time for a constant volume of acetic acid solution with an initial pH of 4 with the stone samples immersed. We found that the protective effects of ALD alumina coatings were extremely promising, slowing the average rate of pH evolution significantly. The eventual failure of the ALD coatings during immersion was also investigated, with interesting morphological findings that point to the role of defects in the coatings, suggesting new directions for improving the use of ALD coatings in future research and applications.

Keywords: protective conservation; atomic layer deposition; cultural heritage

Citation: Boyce, G.P.; Sreenilayam, S.; Balliana, E.; Zendri, E.; Phaneuf, R.J. Amorphous Alumina ALD Coatings for the Protection of Limestone Cultural Heritage Objects. *Coatings* **2024**, *14*, 931. https://doi.org/10.3390/coatings14080931

Academic Editors: Mingheng Li and Yong X. Gan

Received: 14 June 2024
Revised: 21 July 2024
Accepted: 22 July 2024
Published: 25 July 2024

1. Introduction

While commonly considered to be a long-lasting and resilient material, limestone is often subjected to hazards that can threaten its longevity. Of these hazards, the past and recent literature suggest that environmental pollution has been and remains the most significant [1–4]. In past decades, a typical pattern of limestone degradation from environmental pollution presented as black crusts of gypsum, $CaSO_4 \cdot 2H_2O$, formed when SO_2 from acid rain and particulates reacts with calcium carbonate. These black crusts are well documented on limestone across Europe and correlate compositionally to human-generated pollutants in the environment [5–7]. Today, this decay pattern has become less of a concern due to SO_2 emissions being severely limited in western Europe since the 2000s [8,9]. Instead, other pollutants such as NO_2, which overall remains at high levels [10], and CO_2, which continues to increase in concentration globally [11], present larger threats. The effects of these pollutants on limestone are still being investigated but are of significant concern for their potential to increase rain acidification and promote stone washout.

Istria stone, the limestone investigated throughout this work, was chosen because it is both specific to the interests of cultural heritage conservation and representative of compact carbonate stones in general. As it relates to cultural heritage, Istria stone is commonly

used as a building material throughout Venice, Italy, and has unique decay patterns due to the stone's morphology and the local environment in the Venetian lagoon. Istria stone is a low-porosity (<1%), compact stone, which allows it to be relatively resistant to the harsh marine environment [12]. Because of its compactness, the decay patterns are mainly localized to the stone's surface and tend to only penetrate the bulk by water infiltration in clay veins, clay swelling, and stone piece detachments [13]. More recent work focusing on deterioration patterns of Istria stone in connection with local environmental conditions during the years 2000–2020 has revealed that the air pollutant of most significant concern now in Venice is NO_2 produced by water traffic [14]. Additionally, for the entire Veneto region, the abundance of PM_{10} pollutants frequently exceeds the limits set by the European air quality directives [15]. The negative effects of air pollutants are exacerbated by the climate of Venice, which has high levels of humidity that cause particulates to remain in the environment for long periods of time. The prolonged presence of pollutants favors potential chemical interactions between particulate matter and stone surfaces. For these reasons, Istria stone makes for a relevant case study to examine ALD's protective effects on stone cultural heritage.

In addition, Istria stone is representative of compact carbonate stones in general, which allows this work to be applicable beyond the cultural heritage conservation field. Protecting stone against deterioration (pollution-induced or otherwise) is relevant for many fields including civil and industrial engineering. In this way, broader conclusions may be drawn from this work to include a variety of stone applications.

Currently, many of the treatments used to protect stone function as water repellents, and work by preventing the infiltration of water by reducing the hydrophilicity of the materials [16,17]. Common treatments include a variety of acrylic polymers that are applied to the stone surface [18]. When applied to stone, these products can also mitigate the incursion of acids, salts, and biological organisms, all of which can otherwise be carried to the stone's surface by water and provide pathways for degradation. However, these polymer treatments are not without drawbacks. Specifically, acrylic polymers tend to suffer from photo-degradation, which limits their durability and effectiveness over time [19]. Moreover, polymer treatments do not always achieve uniform and conformal coverage across a stone's topographical features, potentially providing uneven protection [20]. Consequently, examining novel protective solutions that can address the durability and the unique morphological characteristics of stone cultural heritage is of great interest and the focus of this work.

Atomic layer deposition (ALD) is a thin-film fabrication technique ubiquitous in the microelectronics industry for its application of high-quality and conformal films that may be grown with angstrom-level control [21]. The ALD process uses vapor-phase precursors in a sequential manner to react with a surface in a self-limiting way. In theory, the self-limiting nature of the reactions allows a single atomic layer to be grown with each cycle of the process. A great variety of film compositions and crystallographic structures may be grown with ALD by varying the temperature and the type of precursors used [22]. Perhaps the most studied of these compositions is amorphous alumina, Al_2O_3, which is considered a model system due to efficient and entirely self-limiting chemical reactions as well as the strong nature of Al-O bonds [23]. Finally, although films of similar compositions can also be produced using molecular beam epitaxy (MBE) [24] or chemical vapor deposition (CVD) [25] ALD has the advantage of the potential for unmatched conformality owing to the self-limiting nature of the individual reaction steps.

Figure 1 shows one complete, ideal cycle of ALD alumina growth. The process can be explained as follows: First, the substrate surface, which is assumed to be uniformly hydroxylated, is exposed to a pulse of the gaseous precursor tri-methyl-aluminum (TMA). The TMA reacts with surface hydroxyl groups, resulting in chemisorbed $(CH_3)_2AlO$, and physisorbed TMA [26]. The second step is a purge in which the excess TMA and methane are removed from the system with the help of a flux of inert carrier gas. In the third step, a second precursor is introduced: water vapor is flowed into the chamber and reacts with the

the surface methyl groups, generating methane gas along with a monolayer of hydroxyl groups on the aluminum oxide coated sample surface. The fourth step is another purge to remove the excess water and methane. Because the cycle ends with a uniform surface of hydroxyl terminations, similar to the start of the cycle, the process may be continuously repeated for layer-by-layer growth. While this idealized picture may be realized to some extent experimentally, several factors introduce limits to the model. Notably, in the first step of the cycle, a uniform layer of hydroxyl terminations is assumed. However, the extent to which this homogeneity can be realized experimentally depends upon the substrate's composition and how the surface is treated prior to deposition. Defects, particularly impurities on the surface, may create sites where reaction does not occur. Additionally, steric hindrance of the precursor gases can allow ligands to block potential surface reaction sites during deposition, also leading to defects [27]. When incomplete surface reactions occur, it is likely that the ALD process will not proceed with ideal layer-by-layer growth but rather follow an island nucleation and coalescence model [28]. With this model, material is deposited selectively only on sites that are available for reaction, creating an initial islanded morphology. As more ALD cycles are applied, the islands eventually grow and coalesce to form a nearly conformal, contiguous film. However, incomplete coalescence will result in extended defects analogous to grain boundaries, which can act as paths for relatively fast permeation through the film. Finally, we note that careful studies by Naumann et al. [29] for ALD alumina on silicon and by Young et al. [30] for ALD alumina on carbon nanotubes show that the films are oxygen rich for the smallest thicknesses and suggest that they approach the ideal Al_2O_3 stoichiometry only for relatively thick films, when the number of growth cycles reaches a few hundred cycles, depending on substrate and growth temperature.

surface methyl groups, generating methane gas along with a monolayer of hydroxyl groups on the aluminum oxide coated sample surface. The fourth step is another purge to remove the excess water and methane. Because the cycle ends with a uniform surface of hydroxyl terminations, similar to the start of the cycle, the process may be continuously repeated for layer-by-layer growth. While this idealized picture may be realized to some extent experimentally, several factors introduce limits to the model. Notably, in the first step of the cycle, a uniform layer of hydroxyl terminations is assumed. However, the extent to which this homogeneity can be realized experimentally depends upon the substrate's composition and how the surface is treated prior to deposition. Defects, particularly impurities on the surface, may create sites where reaction does not occur. Additionally, steric hindrance of the precursor gases can allow ligands to block potential surface reaction sites during deposition, also leading to defects [27]. When incomplete surface reactions occur, it is likely that the ALD process will not proceed with ideal layer-by-layer growth but rather follow an island nucleation and coalescence model [28]. With this model, material is deposited selectively only on sites that are available for reaction, creating an initial islanded morphology. As more ALD cycles are applied, the islands eventually grow and coalesce to form a nearly conformal, contiguous film. However, incomplete coalescence will result in extended defects analogous to grain boundaries, which can act as paths for relatively fast permeation through the film. Finally, we note that careful studies by Naumann et al. [29] for ALD alumina on silicon and by Young et al. [30] for ALD alumina on carbon nanotubes show that the films are oxygen rich for the smallest thicknesses and suggest that they approach the ideal Al_2O_3 stoichiometry only for relatively thick films, when the number of growth cycles reaches a few hundred cycles, depending on substrate and growth temperature.

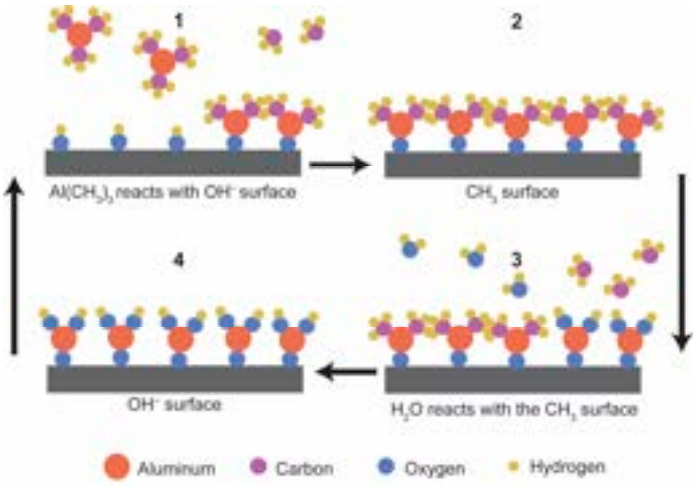

Figure 1. Schematic of one complete, ideal cycle of ALD alumina growth.

ALD metal oxide films are interesting candidates for the protection of cultural heritage for a few reasons. First, the application of ALD is extremely precise in terms of the thickness of the film deposited on a substrate due to the self-limiting nature of the chemical reactions and the ability to precisely control how many cycles are applied [23]. In principle, the efficacy of a perfect coating is limited by its thickness, at least within the diffusion limit as described by Fick's laws, with thicker coatings offering better protection [31]. However, a coating that is too thick can produce a change in the appearance of an object by imparting color or changing the topography. Applying coatings that are extremely thin can mitigate these potential issues, but traditional application methods for coating cultural heritage objects such as spray coating or brushing are limited in this aspect of precision. The lack of precision can result in material buildup in areas of overlap or incomplete coverage on shadowed or difficult to reach regions. In contrast, ALD-applied coatings ideally have a consistent and controllable thickness on all wettable surfaces, assuming adequate time is given for the precursors within the reaction chamber to surround and adsorb to the object.

A second aspect that makes ALD interesting for cultural heritage is the ability to create coatings with extreme conformality, allowing for nearly complete and uniform coverage on substrates with complex topography and high-aspect-ratio pores [32,33]. Conformality of coatings is important for both uniform protection of an object and maintaining a uniform appearance. Bare or unevenly thin regions allow fast permeation pathways to the underlying substrate, compromising the effectiveness of the treatment. In addition, the bare and uneven regions can produce a non-uniform appearance if the coating is within a thickness range that is able to be seen, by showing contrast between the coated and bare regions. This is important for cultural heritage applications because not altering an object's appearance is a priority for protective interventions. ALD is particularly interesting in this regard because in the absence of thin-film interference effects, many ALD metal oxide films are transparent and colorless, including the alumina coatings applied in this work.

Finally, ALD has proven to be an incredibly versatile method of protection, showing successful results in protecting a wide range of materials from diverse degradation mechanisms. For examples, ALD films have been shown to be effective at preventing the tarnishing of silver objects [34] and slowing the aqueous alteration of glass [35]. Finally, they are capable of dramatically slowing acid attack of limestone, which is the focus of this work and, to the best of our knowledge, the first report of its kind. For these reasons, ALD treatments are potentially very attractive for the cultural heritage field.

However, there are a few limitations on ALD's application to cultural heritage. Perhaps the most apparent limitation for stone is the size of monumental stone objects relative to that of available reaction chambers. Using currently available commercial reactors, ALD would only be applicable for smaller objects and fragments or for larger works that can be disassembled and reassembled, such as mosaics or stone cover slabs. There is certainly interest in creating larger-format ALD reaction chambers and scaling up the size of substrates available for ALD [36]. Currently, however, large-format commercially available ALD chambers are mainly designed for photovoltaic applications; this has resulted in the production of large-area and short-height chambers that, while large in total volume, do not have the correct dimensions to admit a larger object such as a stone sculpture [37]. Nevertheless, the technology for scaling up the ALD process is growing and could potentially be adapted to the needs of cultural heritage if a desire is present in the future.

A related limitation is the cost of ALD. The high upfront cost of the specialized instrumentation, as well as the high cost of the consumable precursor gasses, can make employing this technique a large investment, which can limit its use in a museum setting.

Finally, the temperature required for the ALD process is important to consider for cultural heritage applications. ALD growth is based on thermally activated reactions, and so the properties of the resulting films can be quite sensitive to the temperature at which the depositions occur [38]. For cultural heritage, a deposition temperature must be compatible with the cultural object for which it is being used. For amorphous alumina ALD films, 150 °C (the temperature used in this work) is considered well within the temperature range for favorable growth [23]. It has been suggested that amorphous alumina has a large acceptable temperature range due to the high exothermicity of the Al_2O_3 ALD surface reactions, with one study showing depositions as low as room temperature with only minor changes in the growth thickness per cycle [39]. Despite the promising results two decades ago, more research on ALD in the low-temperature regime (<100 °C) is severely lacking. While an exploration of lowering the ALD temperature is not the focus of this work, it is the focus of our future investigations on ALD for the protection of cultural heritage. These temperature investigations are important for a more complete picture of ALD films as a protective method for stone because it is known that the strain behavior and mechanical properties of stone can irreversibly change at temperatures above that of the ambient [40]. In addition, low deposition temperatures mitigate potential thermal stresses that can be introduced with the cooling of coated objects when the coating and object have different coefficients of thermal expansion [41]. Further, to broaden the range of ALD

applications in general to polymeric materials or biomaterials, more rigorous explorations of low-temperature ALD are necessary.

In this work, we examine the potential of ALD coatings as protective barriers to mitigate reactions with harmful particulates and acid rain and consider the aspects of such a protective conservation treatment specific to cultural heritage objects. Considering that the conditions of pollution-induced stone deterioration are complex and impossible to exactly replicate in a laboratory setting, we chose to implement a simple acidic aqueous immersion method that is amenable to in situ monitoring. In this way, we explored the efficacy of ALD alumina coatings in protecting limestone broadly from acidic aqueous solutions.

2. Materials and Methods

2.1. Sample Preparation

Istria stone is used throughout this work as a case study to test the effects of applying protective ALD alumina coatings to limestone. Istria stone is very compact with an open porosity of less than 1%. A typical chemical composition of Istria stone is calcium carbonate with MgO, SiO_2, Fe_2O_3, and Al_2O_3 impurities as well as microfossils [42]. Samples were cut from slabs of Istria stone into 1 cm cubes and polished with 180, then 320 grit silicon carbide paper. They were then rinsed in deionized water and allowed to dry at room temperature. The samples had final masses of 2.50 ± 0.25 g.

The amorphous alumina ALD films were grown on the Istria stone samples using a Beneq TFS 500 Atomic Layer Deposition (ALD) system (Beneq, Espoo, Finland), in a class 1000 clean room. TMA and H_2O were used as the precursors, with 2 s pulses for each. N_2 was used for 2 s purges. All the films in this work were grown at 150 °C for 50, 250, or 500 cycles of deposition. Samples were allowed to equilibrate within the chamber for at least 30 min prior to deposition. Within the reaction chamber, custom holders were used to support the samples by three points of contact. The samples were flipped halfway through the depositions to mitigate any defects caused by contact with the holders.

2.2. Reflectance and Colorimetry

To examine any changes in the appearance of the Istria stone from applying the ALD alumina coatings, spectrophotometric and colorimetric measurements were performed. Measurements were taken from 3 spots on 7 samples for each condition: uncoated samples, hereafter referred to as 'No-ALD samples', and samples treated with 50 cycles, 250 cycles, and 500 cycles of ALD, hereafter referred to as 'ALD samples.' The colorimetric coordinates in CIE 1976 $L^*a^*b^*$ were acquired with a Konica Minolta CM-700d spectrophotometer (Konica Minolta, Tokyo, Japan) (illuminant D65, observer 8-degree viewing angle geometry) and analyzed with Spectra Magic NX 6 software. The equations used for calculating the average chromatic coordinates and the associated uncertainty are as follows:

$$L^* = \frac{\sum_{i=0}^{N} L_i^*}{N}, \tag{1}$$

where N is 21 from the measurements of 3 spots on 7 samples for each condition. a^* and b^* are calculated similarly.

$$\sigma_{L^*}{}^2 = \frac{\sum_{i=0}^{N} \left(L_i^* - \overline{L^*}\right)^2}{N}, \tag{2}$$

The change in the chromatic coordinates and associated uncertainties were calculated with the following equations:

$$\Delta L^* = L^*_{ALD} - L^*_{no\ ALD}, \tag{3}$$

Δa^* and Δb^* are calculated similarly.

$$\sigma_{\Delta L^*}{}^2 = \sigma_{L^*_{ALD}}{}^2 + \sigma_{L^*_{no\ ALD}}{}^2, \tag{4}$$

$\sigma_{\Delta a}$ and $\sigma_{\Delta b}$ are calculated similarly.

$$\Delta E = \sqrt{\Delta L^{*2} + \Delta a^{*2} + \Delta b^{*2}}, \quad (5)$$

$$\sigma_{\Delta E}{}^2 = \left(\frac{\Delta L^{*2}}{\Delta L^{*2} + \Delta a^{*2} + \Delta b^{*2}} * \sigma_{\Delta L}{}^2\right) + \left(\frac{\Delta a^{*2}}{\Delta L^{*2} + \Delta a^{*2} + \Delta b^{*2}} * \sigma_{\Delta a}{}^2\right) + \left(\frac{\Delta b^{*2}}{\Delta L^{*2} + \Delta a^{*2} + \Delta b^{*2}} * \sigma_{\Delta b}{}^2\right). \quad (6)$$

According to the literature, the limit for a chromatic variation to be considered visually insignificant is $\Delta E < 3$, while chromatic variations of $\Delta E > 5$ are considered significant and are not suitable for cultural heritage interventions [43,44].

2.3. FTIR-ATR

Because the presence of ALD alumina films on the Istria stone is not evident by visual inspection, it was necessary to confirm the presence of the coating with spectroscopic methods. Typically, the presence and thickness of ALD thin films are verified using spectroscopic ellipsometry. However, this technique is best suited for optically flat wafer substrates (e.g., Si, GaAs, and Ge) [45]. Due to the highly rough nature of the stone substrates, this method would not produce meaningful data regarding the presence or thickness of the ALD alumina films. FTIR-ATR was used instead to analyze the presence of alumina on the surface of Istria stone samples with increasing numbers of ALD cycles applied.

A portable ALPHA II spectrometer by Bruker Optics® (Bruker, Billerica, MA, USA) equipped with an ATR modulus with a single-bounce diamond was used to collect the spectra. Spectra acquired in the range between 4000 and 400 cm^{-1} were obtained by collecting 250 scans with 4 cm^{-1} spectral resolution. These measurements were taken for 7 samples, in 1 spot each, for each condition (No ALD and 50 cycles, 250 cycles, and 500 cycles of ALD).

A semi-quantitative analysis of the ALD alumina coating was performed as follows. The spectra were normalized to the well-defined calcite peak at 867 cm^{-1} according to the equation:

$$a_{norm}(w) = a(w) * \frac{1}{a(867\ cm^{-1})} \quad (7)$$

where a = absorbance and w = wavenumber. Then, the spectra for each condition (No ALD and 50 cycles, 250 cycles, and 500 cycles of ALD) were averaged and a standard deviation was taken. Using an absolute baseline, the peak height at 920 cm^{-1}, which is an Al-O longitudinal optic (LO) mode [46], was measured. In addition, numerical integrations were performed using the trapezoidal method and an absolute baseline in the range 978–891 cm^{-1} for each of the normalized spectra. The areas resulting from the integrations were also averaged, and the standard deviation was taken.

These points are representative of the Al-O signal in comparison with the C-O signal and were taken as indicative of the concentration of ALD alumina coating present on the calcium carbonate surface. The values obtained from this analysis were then graphically related to the number of ALD cycles.

2.4. Aqueous Acid Immersion and pH and pCa Tracking

To characterize how well the ALD coatings protect the Istria stone from acid attack, samples with and without ALD were immersed in 100 mL of an aqueous solution of acetic acid with a starting pH of 4 while stirring. A pH of 4 was chosen to approximate the conditions of severe acid rain. Of the coating thicknesses studied in this work, ALD films resulting from 500 cycles, corresponding to approximately 90 nm, were chosen for the immersion experiments as providing good visual appearance and the highest likely effectiveness of protection against acid attack based on preliminary experiments.

A Crison GLP 21 pH meter (Crison Instruments, Alella, Spain) was used to continuously measure the pH of the acid immersion solution. This was used as a method to track how much limestone was available for reaction with the acid.

Additionally, aliquots of acid solution from the acid immersion experiments were analyzed for Ca^{2+} ion concentration with a Perkin Elmer Optima 5300SV Inductively Coupled Plasma Optical Emission Spectrometer (ICP-OES) (PerkinElmer, Waltham, MA, USA). The [Ca^{2+}] was quantified by means of a seven-point calibration curve with acetic acid solution used as the diluent. For the samples with no ALD coating, 5 mL aliquots were collected from the immersion experiment at each 0.5 increase in pH. For the ALD-coated samples, the aliquot collection intervals were less regular because of the long duration of the immersion experiments, spanning days and nights. Aliquots for these samples were collected as regularly as possible, but with up to pH $\pm$ 1.0 variance in the collection interval for some samples.

To make a comparison to pH, pCa was calculated from the Ca^{2+} concentration data according to the equation:

$$pCa = -\log_{10}[Ca^{2+}], \quad (8)$$

For additional analysis, the pCa data for each condition (500 cycles of ALD and no ALD) were averaged using linear interpolation and graphically related to pH data treated in the same way. One standard deviation was used in estimating the uncertainties.

2.5. Optical Microscopy

A Dino-Lite digital microscope AM4113 series (VIDY OPTICAL (WUXI) CO., LTD., Wuxi, China) was used for optical imaging of the samples throughout the experiments. All samples were analyzed after the ALD coating was applied. The samples that were immersed in acid were rinsed in deionized water and allowed to dry at room temperature, then analyzed with the digital microscope again. Some of the samples were briefly examined during the acid immersion; these samples were taken out of the acid solution at various times and dried with paper before being quickly imaged and returned to the acid solution. Two different magnifications, namely, x25 and x50, were used throughout the analyses.

2.6. SEM-EDX

An FEI Quanta 200 Scanning Electron Microscope (SEM) (FEI company, Hillsboro, OR, USA) equipped with an EDAX Element-C2B Energy Dispersive X-ray (EDX) detector was used to examine the morphological characteristics and the presence and distribution of aluminum for various samples. No-ALD samples with and without acid immersion as well as 500-cycle ALD-coated samples with and without acid immersion were examined.

3. Results and Discussion

3.1. Appearance Changes

The applied ALD alumina films in this work are transparent across the visible part of the electromagnetic spectrum; however, changes in color can arise from thin-film interference and scattering effects. As light passes through the ALD film and reflects from the substrate surface, constructive or destructive interference can occur as described by the Fresnel equations [47]. According to the refractive index of the film and substrate, the film thickness, and the angle of incidence of light, color changes from applying the ALD coating may be present. In addition, coatings that make a rough surface smoother and have an index of refraction intermediate between that of the substrate and that of air can partially suppress light scattering. Alternatively, if the coating increases roughness, light scattering will increase.

Slight variations in the color of the Istria stone from sample to sample made distinguishing the change in appearance due to the ALD coating challenging. Figure 2 shows the resulting average reflectance spectra of Istria stone samples with no ALD and 50 cycles, 250 cycles, and 500 cycles of ALD alumina applied. While systematic differences are evi-

an index of refraction intermediate between that of the substrate and that of air can partially suppress light scattering. Alternatively, if the coating increases roughness, light scattering will increase.

Slight variations in the color of the Istria stone from sample to sample made distinguishing the change in appearance due to the ALD coating challenging. Figure 2 shows the resulting average reflectance spectra of Istria stone samples with no ALD and 50 cycles, 250 cycles, and 500 cycles of ALD alumina applied. While systematic differences are evident, the statistical variance in the average reflectance spectra of the No ALD samples is larger than any differences seen from applying the ALD alumina coating. This is nevertheless an interesting result because it shows that applying the ALD coating results in a change in appearance comparable to the differences that are already present from stone to stone.

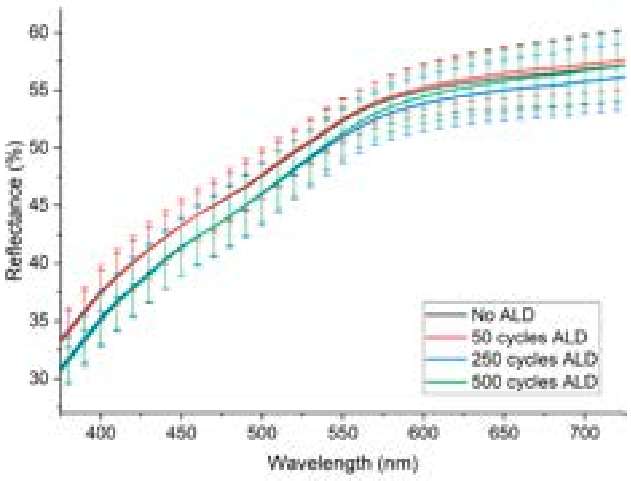

Figure 2. Average reflectance spectra of Istria stone samples with increasing numbers of ALD alumina cycles applied.

Measurements of the colorimetric coordinates in CIE 1976 $L^*a^*b^*$ were used to calculate the average chromatic variation from applying the ALD alumina coatings. The results of these calculations are shown in shown in Figure 3. As with the average reflectance spectra, a large statistical variance is present from the variety in individual stone samples' appearances. Again, despite the large variance, there are systematic trends present in the data. Most importantly, the calculated average ΔE values are <1.5, indicating a non-visible color change [43,44]. For all ALD conditions tested, the calculated average ΔE values and their associated uncertainties are <5 and confirm the visual impression that the application of the ALD films is not perceivable by eye. Again, despite the difficulty in isolating the effects of the ALD film in a statistically significant way, this result shows that any change in appearance caused by the application of these particular ALD alumina films to Istria stone is below the generally accepted standards for cultural heritage interventions.

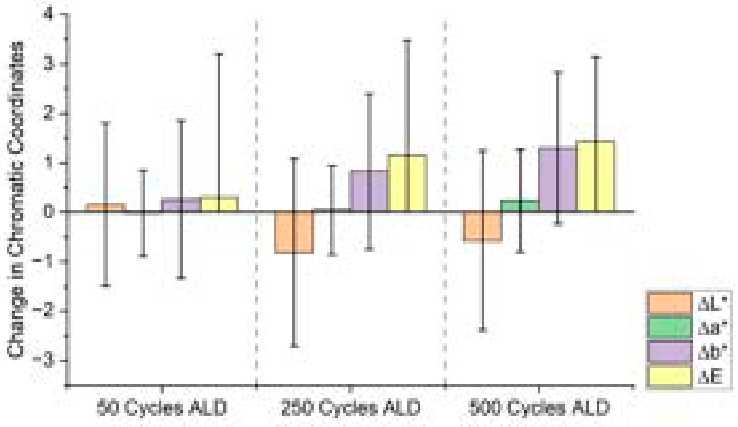

Figure 3. Average change in chromatic coordinates (specular component included) of Istria stone from applying 50, 250, and 500 cycles of ALD alumina.

In addition, the colorimetric measurements showed that for all thickness conditions the total reflectance (specular component included) values and the diffuse reflectance (specular component excluded) values were nearly identical. The similarity indicates that there is likely no change in the morphology of the stone surface from the ALD coatings contributing to appearance changes [48].

3.2. Verifying the Presence of ALD Alumina with FTIR-ATR

Because the ALD coatings were invisible to the eye, FTIR-ATR was used to confirm

Figure 3. Average change in chromatic coordinates (specular component included) of Istria stone from applying 50, 250, and 500 cycles of ALD alumina.

In addition, the colorimetric measurements showed that for all thickness conditions the total reflectance (specular component included) values and the diffuse reflectance (specular component excluded) values were nearly identical. The similarity indicates that there is likely no change in the morphology of the stone surface from the ALD coatings contributing to appearance changes [48].

3.2. Verifying the Presence of ALD Alumina with FTIR-ATR

Because the ALD coatings were invisible to the eye, FTIR-ATR was used to confirm their presence on the Istria stone samples. A semi-quantitative method as described in the methods section was used to analyze the FTIR spectra for samples with increasing numbers of ALD cycles. Figure 4a shows the average spectra with associated uncertainty for samples with no ALD, 50 cycles of ALD, 250 cycles of ALD, and 500 cycles of ALD, all normalized to the calcite peak at 867 cm^{-1}. The peak ~920 cm^{-1} is an Al-O longitudinal optic (LO) mode [46] and is indicative of the presence of the ALD alumina coating. As expected, there was an increase of the Al-O peak height and integrated intensity with increasing numbers of ALD cycles, as illustrated in Figure 4b. The sublinear dependence is qualitatively consistent with the response of the FTIR-ATR probe, which weights contributions from deeper regions less strongly.

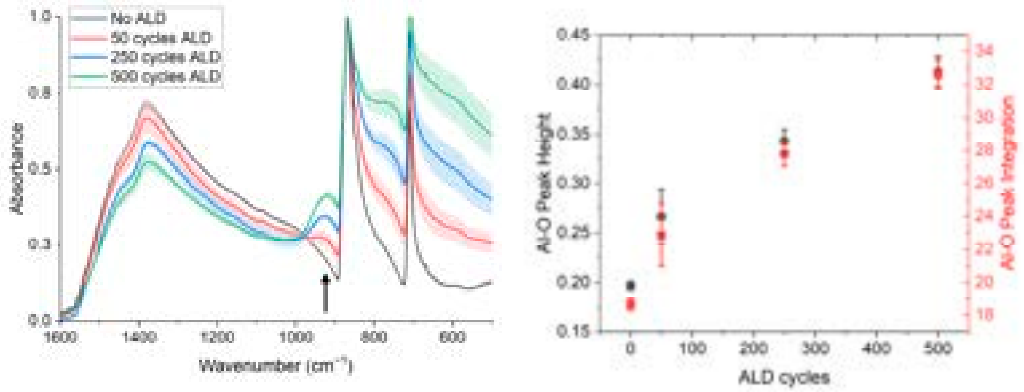

(**a**) (**b**)

Figure 4. (**a**) Average FTIR-ATR spectra of Istria stone samples with no ALD and 50 cycles, 250 cycles, and 500 cycles of ALD; the arrow indicates the Al-O longitudinal optic (LO) mode peak position, near 920 cm^{-1}. (**b**) The height of Al-O absorbance (black circles) and the integrated peak intensity (red squares) with increasing numbers of cycles of ALD alumina.

3.3. Morphology and Homogeneity of the ALD Coatings on Istria

SEM was used to visualize any morphological changes in the stone surface as a result of applying the ALD coating. As can be seen in Figure 5, the morphology of the stone did not change significantly with the application of 500 cycles of ALD alumina. In fact, no apparent morphological differences were perceptible at 500× magnification, as in Figure 5a,c. At higher magnification, 4000×, as in Figure 5b,d, some slight differences in morphology could be detected; overall, the ALD-coated samples appeared slightly smoother, with some of the calcium carbonate grains less distinct. However, these differences appeared to be extremely subtle and supported the reflectance and colorimetric findings that the appearance of the stone surfaces was not altered by morphological changes from application of the ALD coating.

In addition, SEM-EDX was performed to characterize the presence and distribution of ALD coating. The elemental aluminum signal was found to be very uniform over the ALD-treated surfaces. Point spectra were taken across various areas with diverse morphological features, such as the smoother regions and the distinct calcium carbonate grains for the ALD coated samples resulting in an average Al wt% of 7.2 ± 1.0. These spectra showed consistent Al wt% signal across the differing features, indicating that the ALD alumina was dispersed homogenously and was not preferentially located in specific areas defined by morphology, such as the smooth or textured areas. The SEM-EDX are is provided in

SEM was used to visualize any morphological changes in the stone surface as a result of applying the ALD coating. As can be seen in Figure 5, the morphology of the stone did not change significantly with the application of 500 cycles of ALD alumina. In fact, no apparent morphological differences were perceptible at 500× magnification, as in Figure 5a,c. At higher magnification, 4000×, as in Figure 5b,d, some slight differences in morphology could be detected; overall, the ALD-coated samples appeared slightly smoother, with some of the calcium carbonate grains less distinct. However, these differences appeared to be extremely subtle and supported the reflectance and colorimetric findings that the appearance of the stone surfaces was not altered by morphological changes from application of the ALD coating.

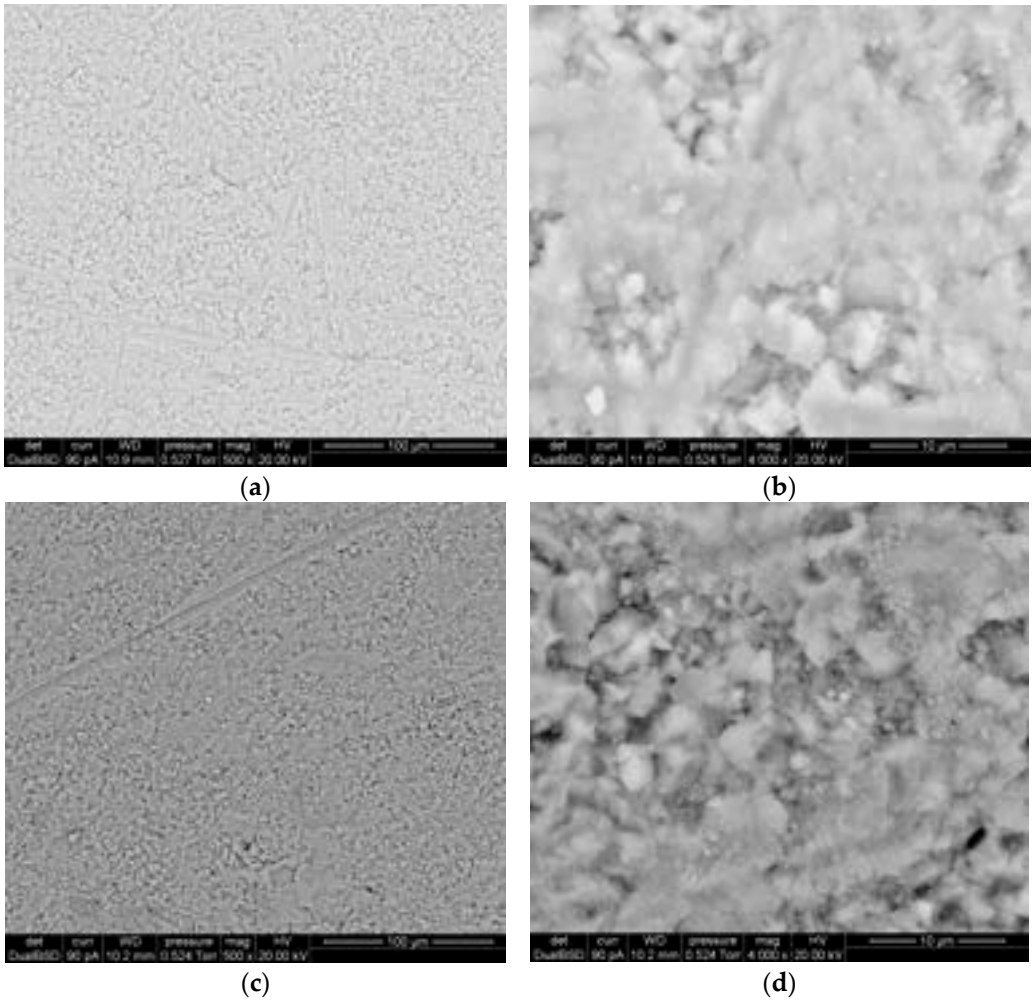

Figure 5. SEM micrographs showing the morphology of (**a**) a No-ALD sample at 500× magnification; (**b**) a No-ALD sample at 4000× magnification; (**c**) a 500-cycle ALD-coated sample at 500× magnification; (**d**) a 500-cycle ALD-coated sample at 4000× magnification. Scale bars are indicated in each panel: 100 µm for panels (**a**,**c**) and 10 µm for panels (**b**,**d**). The images capture backscattered electrons.

In addition, SEM-EDX was performed to characterize the presence and distribution of ALD coating. The elemental aluminum signal was found to be very uniform over the ALD-treated surfaces. Point spectra were taken across various areas with diverse morphological features, such as the smoother regions and the distinct calcium carbonate grains for the ALD coated samples resulting in an average Al wt% of 7.2 ± 1.0. These spectra showed consistent Al wt% signal across the differing features, indicating that the ALD alumina was dispersed homogenously and was not preferentially located in specific areas defined by morphology, such as the smooth or textured areas. The SEM-EDX are in the Supplementary Material, Figures S1 and S2. This finding suggests conformality and homogeneity in the application of the ALD coating and again supports the results from the reflectance and colorimetric measurements, which indicate that the appearance was not noticeably altered by the ALD coating.

For comparison, point spectra for an uncoated Istria sample were also measured and resulted in 0.2 wt% Al signal, supporting the model that the Al wt% measured for the ALD treated samples is almost entirely a result of the ALD alumina coating, not any alumina deposits within the limestone.

3.4. pH Evolution to Measure Protection against Acid Attacks

To characterize how well the ALD alumina coatings protect the Istria stone from acid attack, No-ALD samples and 500-cycle ALD samples were immersed in an aqueous solution of acetic acid with a starting pH of 4 while stirring. For most samples coated with ALD alumina (curves labeled S7–11_ALD), it seems we can locate a point in time for each sample when the ALD coating begins to fail dramatically, as evidenced by a sudden change in the rate of pH evolution with time as seen in Figure 6c.

attack, No-ALD samples and 500-cycle ALD samples were immersed in an aqueous solution of acetic acid with a starting pH of 4 while stirring. For most samples coated with ALD alumina (curves labeled S7–11_ALD), it seems we can locate a point in time for each sample when the ALD coating begins to fail dramatically, as evidenced by a sudden change in the rate of pH evolution with time as seen in Figure 6c.

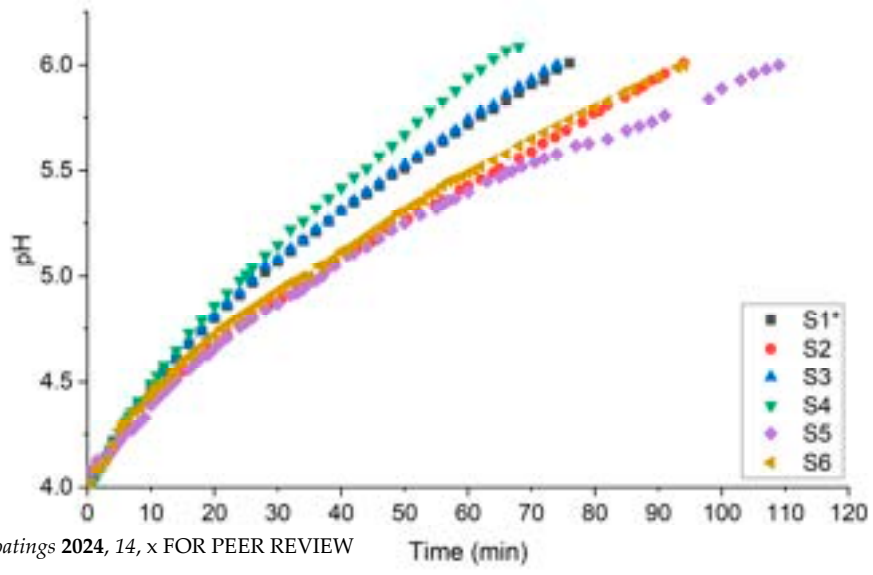

(**a**)

(**b**)

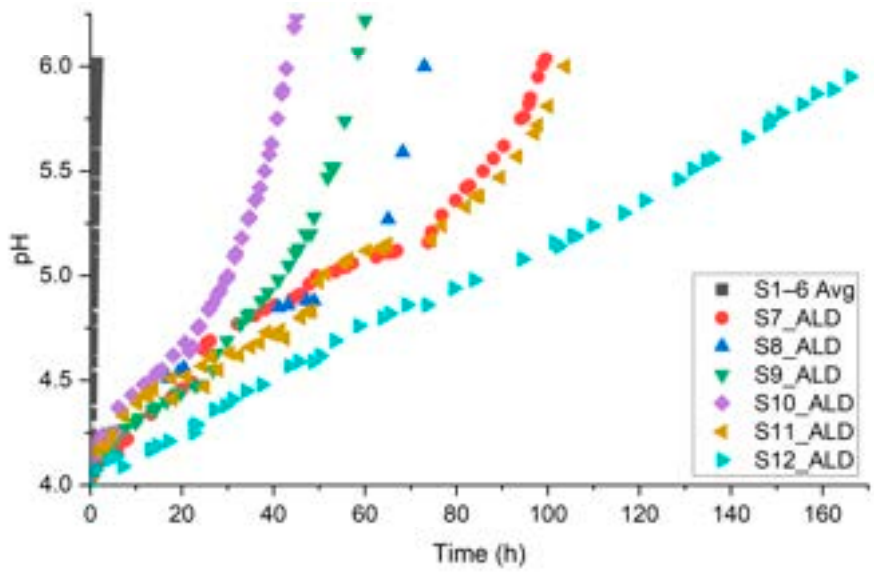

(**c**)

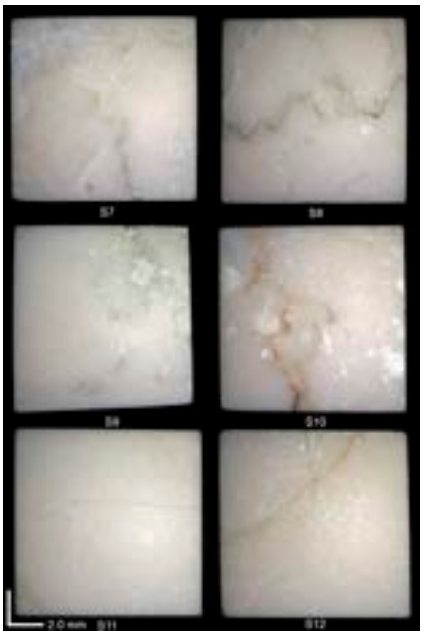

(**d**)

Figure 6. (**a**) pH evolution of acetic acid solution for immersion of the No-ALD samples. (**b**) Optical micrographs, at 25× magnification, of the No-ALD samples after acid immersion. (**c**) pH evolution of acetic acid solution for immersion of the 500-cycle ALD samples. (**d**) Optical micrographs, at 25× magnification, of the 500-cycle ALD samples after acid immersion. * Note that no aliquots were taken from the acid solution for S1 or S7_ALD. This is in contrast to the other samples, S2–6 and S8–12_ALD, in which 3 mL of acid solution was removed at approximately each increment of 0.5 pH increase for ICP-OES analysis.

Figure 6. (**a**) pH evolution of acetic acid solution for immersion of the No-ALD samples. (**b**) Optical micrographs, at 25× magnification, of the No-ALD samples after acid immersion. (**c**) pH evolution of acetic acid solution for immersion of the 500-cycle ALD samples. (**d**) Optical micrographs, at 25× magnification, of the 500-cycle ALD samples after acid immersion. * Note that no aliquots were taken from the acid solution for S1 or S7_ALD. This is in contrast to the other samples, S2–6 and S8–12_ALD, in which 3 mL of acid solution was removed at approximately each increment of 0.5 pH increase for ICP-OES analysis.

While, in general, the dissolution rate of calcite is influenced by a changing pH [49], this alone cannot account for the dramatic change seen for nearly all the ALD-coated samples during the later times of their evolution. Interestingly, the time at which a sudden rate increase initiates varies greatly from sample to sample. The drastic differences can perhaps be explained by the following mechanism of failure. If the mechanism of failure is through small defect sites in the ALD coating, allowing localized sites for the acid to penetrate to the stone and react, then these reaction sites could slowly grow, building up reaction products and eventually leading to faults in the ALD layer and delamination of undercut regions of film due to the action of convection currents. The formation of larger scale faults via outward etching of the film and/or delamination might be indicated by the inflection point in each curve. If the population of defects varies greatly from sample to

While, in general, the dissolution rate of calcite is influenced by a changing pH [49], this alone cannot account for the dramatic change seen for nearly all the ALD-coated samples during the later times of their evolution. Interestingly, the time at which a sudden rate increase initiates varies greatly from sample to sample. The drastic differences can perhaps be explained by the following mechanism of failure. If the mechanism of failure

is through small defect sites in the ALD coating, allowing localized sites for the acid to penetrate to the stone and react, then these reaction sites could slowly grow, building up reaction products and eventually leading to faults in the ALD layer and delamination of undercut regions of film due to the action of convection currents. The formation of larger scale faults via outward etching of the film and/or delamination might be indicated by the inflection point in each curve. If the population of defects varies greatly from sample to sample, which seems likely due to the compositional heterogeneity of Istria stone, then this could result in a large variance when a critical mass of reaction products is reached and when the ALD coating begins to fail dramatically.

Additionally, the natural variation in the Istria stone's chemical composition and morphology may contribute to variation in pH evolution. For example, samples S1, S3, and S4 had prominent silica veins as seen in Figure 6b, which created chemical and morphological heterogeneity. These were the first No-ALD samples for which the acid solution reached a pH of 6 (Figure 6a). This trend also appears to be true for the ALD-coated samples (Figure 6c); S10_ALD had a prominent silica vein and was the earliest of the ALD-coated samples to have its acid solution to reach a pH of 6. In contrast, the last two ALD-coated samples to have the acid solution reach a pH of 6 were S11_ALD and S12_ALD. These two samples showed some heterogeneities in color, as is typical for Istria stone, but overall, the features appeared less diverse than those of S7-10_ALD.

3.5. Optical Imaging

To better understand the mechanism of failure for the ALD-coated Istria stone when subjected to acid attack, the samples were imaged optically after various times in the etching process.

Figure 7 shows the evolution of sample S7_ALD. For this sample, 74 h of immersion directly preceded the inflection point where the rate of pH change began to increase dramatically. However, it is not obvious from visual inspection that a significant change occurred between 74 and 100 h, despite this period corresponding to the fastest rate of pH change. It is clear that calcium acetate reaction products (as verified by FTIR-ATR) were forming on the surface where the ALD coating had selectively failed through the acid exposure, which could be moving the reaction products away from the sites where they are forming rather than allowing them to collect and build up on the surface in a visually apparent way.

Figure 7. Optical micrographs at 50× magnification tracking sample S7_ALD at various times during the etching process.

3.6. ICP-OES Analysis

To complement the in situ method of pH tracking, aliquots of the acid solutions were also collected during the acid immersion experiments and analyzed for Ca^{2+} concentration. The average pH and pCa are presented as a function of time in Figure 8. As expected from the pH tracking, the Ca^{2+} concentration in the solutions with uncoated Istria stone increased much faster than those in the solutions with ALD-coated samples, indicating the significant protective effects of the ALD coating.

3.6. ICP-OES Analysis

To complement the in situ method of pH tracking, aliquots of the acid solutions were also collected during the acid immersion experiments and analyzed for Ca^{2+} concentration. The average pH and pCa are presented as a function of time in Figure 8. As expected from the pH tracking, the Ca^{2+} concentration in the solutions with uncoated Istria stone increased much faster than those in the solutions with ALD-coated samples, indicating the significant protective effects of the ALD coating.

from the pH tracking, the Ca^{2+} concentration in the solutions with uncoated Istria stone increased much faster than those in the solutions with ALD-coated samples, indicating the significant protective effects of the ALD coating.

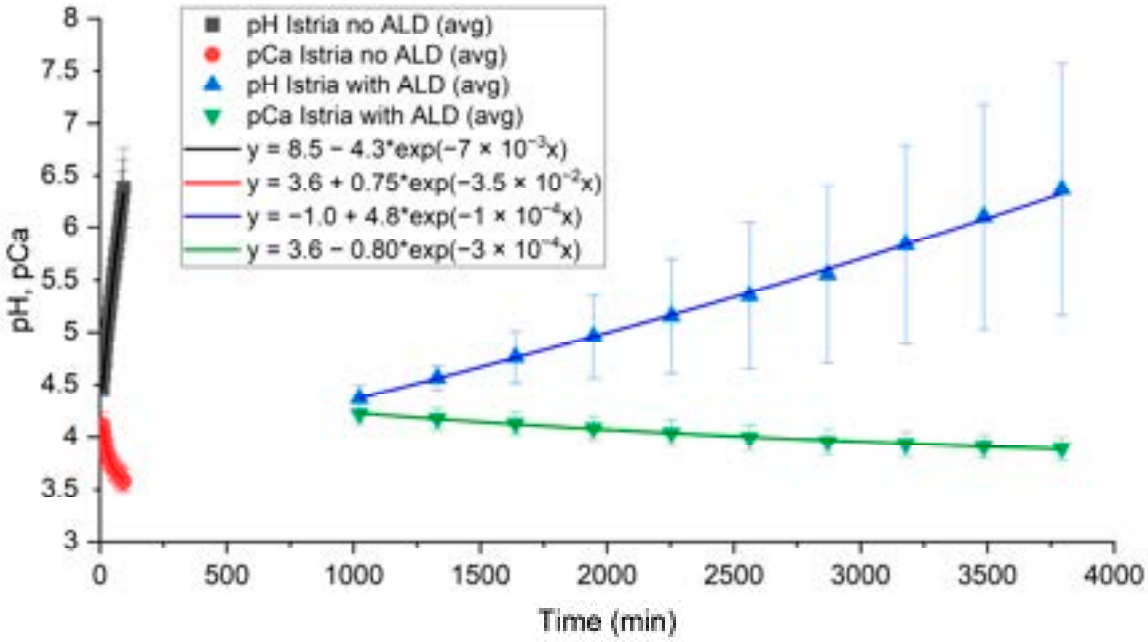

Figure 8. Average pH over time of S2–6 and S8–12_ALD and average pCa over time of S2–6 and S8–10_ALD. Data were averaged using linear interpolation, and the error bars indicate the standard deviation.

Comparing the pH with the pCa over the etching time suggests that there are more contributing factors than simply reactions of acid with calcium carbonate causing a rise in pH over time. Some fraction of the Ca^{2+} almost certainly goes into forming secondary reaction species with low solubility in the acid solution, which settle out to the bottom of the reaction vessel [50] such that the measured rate of change of the pCa does not mirror that of the pH as the former increases.

3.7. Elemental and Morphological Changes from Acid Immersion

The result of the immersion of the No-ALD samples appeared to be mainly an enhanced delineation and rounding of the shape of grains nearly uniformly across the surface as a result of acid etching, as seen by comparing Figure 9a,b. In contrast, the ALD-coated samples that were immersed in acid displayed distinct, approximately circular, pitted features as shown in Figure 9d. It seems there was a selective etching process where the acid has mainly reacted with the stone surface at certain sites, likely beneath defects in the initial ALD film. These defect sites appear to have acted as preferential sites for initiation of pits, which grew outward, nearly isotropically, into pits of various sizes. The variation is likely due to a statistical variation in the time at which each pit nucleated. We discuss the origin of the departure of the pit geometry from isotropy below. For the areas outside of the pitted regions, it appeared the calcium carbonate grains had not evolved in size as seen for the uncoated samples, Figure 9c. Instead, the grain shapes were preserved, suggesting a level of continued protection of the ALD-coated stone outside of the pitted regions.

variation is likely due to a statistical variation in the time at which each pit nucleated. We discuss the origin of the departure of the pit geometry from isotropy below. For the areas outside of the pitted regions, it appeared the calcium carbonate grains had not evolved in size as seen for the uncoated samples, Figure 9c. Instead, the grain shapes were preserved, suggesting a level of continued protection of the ALD-coated stone outside of the pitted regions.

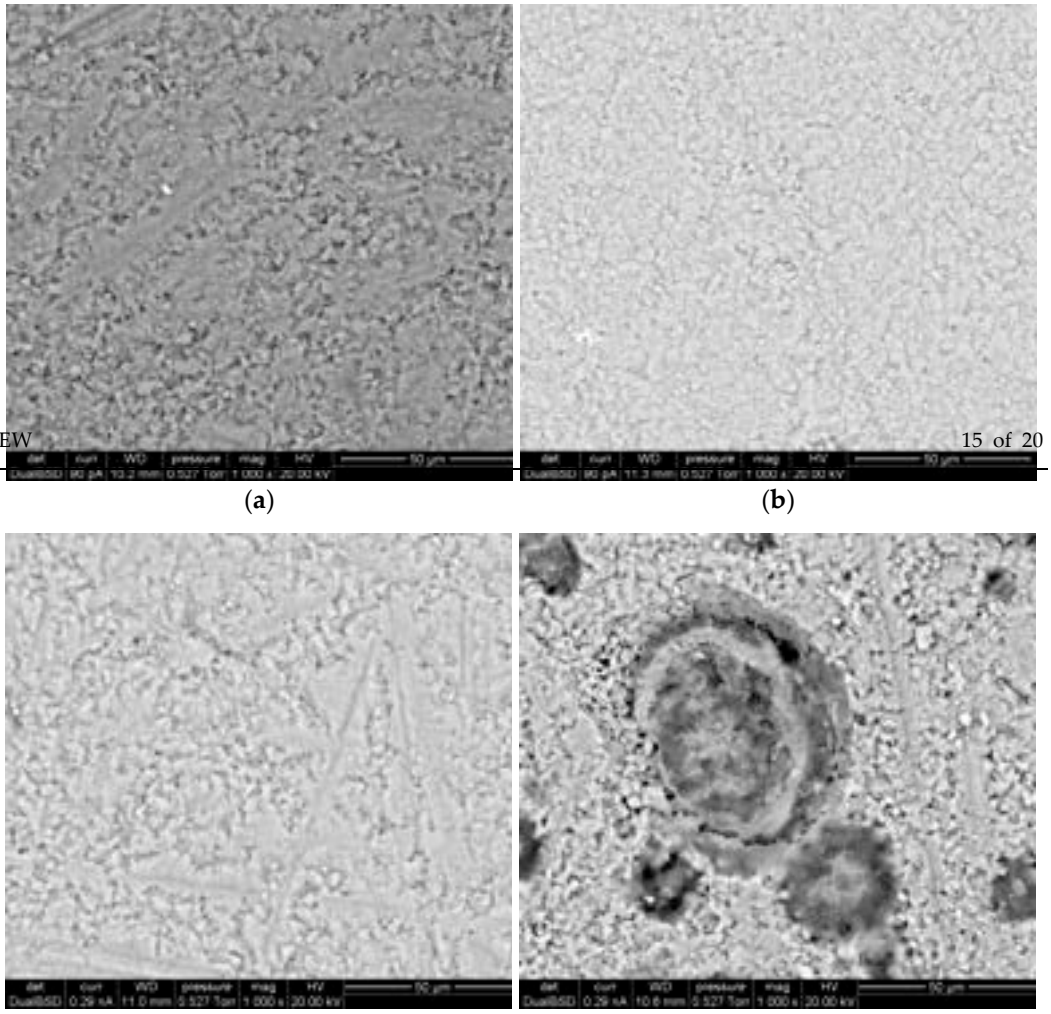

(**a**) (**b**)

(**c**) (**d**)

Figure 9. SEM micrographs at 1000× magnification showing the morphology of (**a**) a No-ALD sample not immersed in acid; (**b**) a No-ALD sample (S7_ALD) immersed in acid; (**c**) a 500-cycle ALD coated sample not immersed in acid; (**d**) a 500-cycle ALD-coated sample (S7_ALD) immersed in acid. Scale bars are indicated in each panel and measure 50 µm for all images. The images capture backscattered electrons.

Surprisingly, elemental mapping with SEM-EDX showed there was a higher Al signal and thus concentration within the pitted regions than outside of the pitted regions, as seen in Figure 10. In the unpitted regions, the Al wt% signal was ~7.0, the same as for the 500-cycle ALD-coated samples, but without acid immersion. This consistent Al wt% signal indicates that the ALD coating in the unpitted regions was still present on the surface even after acid immersion. This finding is consistent with the observation that the ALD-coated calcium carbonate grains outside of the pitted regions did not visibly round during acid exposure (Figure 9d), suggesting that the unpitted regions remained protected by the ALD coating. This is in contrast to the calcium carbonate of the No-ALD sample grains, which did round from the acid immersion Figure 9b. However, within the pitted regions, the Al wt% signal was ~13.8, nearly double the Al wt% signal in the unpitted regions. The most likely explanation for this finding is that the additional aluminum came from the ALD coating; a plausible model was suggested by Willis et al. [51] and involves a series of hydration reactions resulting in an initial reactive dissolution of alumina, followed eventually by reprecipitation of fully hydrated $Al(OH)_3$. The precipitation seemingly occurs at heterogeneous defect sites resulting from the etching of the underlying stone surface, while the dissolution of alumina can be nearly uniform across the surfaces of the ALD alumina coating. This local redeposition results in a departure of the pit shapes from hemispherical, as mentioned above. The model of dissolution and redeposition of the ALD coating is supported by the Pourbaix diagram for alumina dissolution in bulk crystalline form, which predicts instability of alumina outside the pH range of 5.8–7.3 [52]. This instability has also been demonstrated for amorphous alumina ALD films immersed in acidic conditions (1M H_2SO_4) showing eventual dissolution of the alumina ALD film

the ALD alumina coating. This local redeposition results in a departure of the pit shapes from hemispherical, as mentioned above. The model of dissolution and redeposition of the ALD coating is supported by the Pourbaix diagram for alumina dissolution in bulk crystalline form, which predicts instability of alumina outside the pH range of 5.8–7.3 [52]. This instability has also been demonstrated for amorphous alumina ALD films immersed in acidic conditions (1M H_2SO_4) showing eventual dissolution of the alumina ALD film [53].

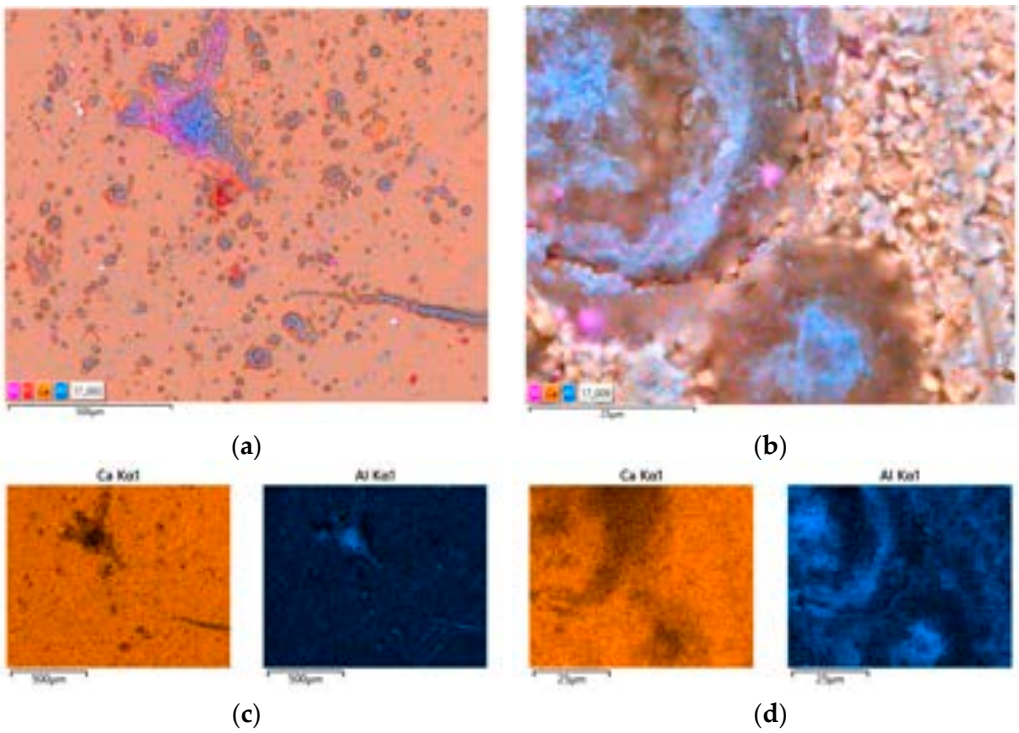

Figure 10. SEM-EDX elemental maps of Istria stone treated with 500 cycles of ALD and immersed in acid (S7_ALD), illustrating the high concentration of elemental aluminum in pitted regions (**a**) at 100× magnification and (**b**) and 2000× magnification. The Ca and Al maps in (**a**,**b**) are illustrated independently in (**c**,**d**) respectively.

The pitted regions were examined at higher magnification to investigate the morphology of the redeposited aluminum-containing species. As shown Figure 11, the visible platelet morphology and the characteristic high elemental aluminum concentration are evidence of aluminum hydroxide $Al(OH)_3$ in the gibbsite form, which has a characteristic platelet structure and readily forms in acidic conditions when Al and OH are present [54–56].

These findings again support the model that a series of hydration reactions resulting in an initial reactive dissolution of amorphous ALD alumina, followed eventually by reprecipitation of fully hydrated $Al_2(OH)_3$, occurs in our system. Further, the finding that pitted regions form and that the gibbsite is localized to these areas suggests that defects in the initial ALD coating play a distinct role in the eventual failure of protection. It seems likely that defects in the ALD coating provide sites for the permeation of the acid to allow access to the underlying stone. The selective etching eventually forms pitted regions, which provide heterogeneous nucleation sites for crystallization of gibbsite, $Al_2(OH)_3$. While exploring the exact mechanisms of ALD alumina dissolution and redeposition as gibbsite in acidic solutions is beyond the scope of this work, the results of this model suggest new avenues for future research; to improve the protective effects of ALD alumina coatings, particular attention must be paid to mitigating defects in the initial ALD film.

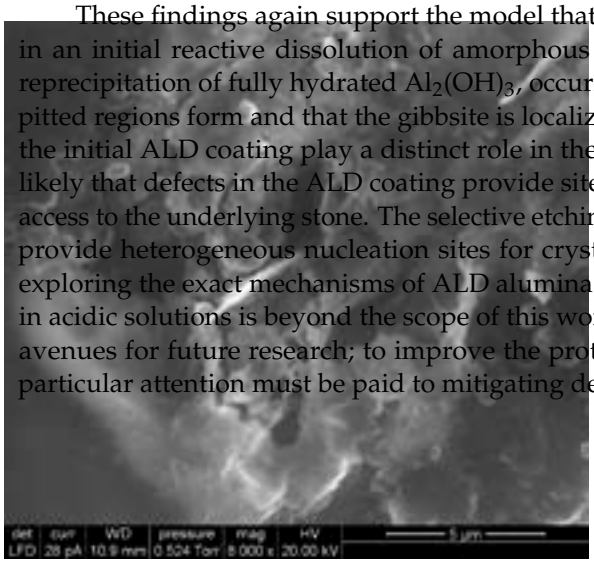

Figure 11. SEM micrograph, at 8000× magnification, of a pitted region of Istria stone treated with ALD alumina (S10_ALD) and immersed in acid solution. The area shown is in a pitted region with high aluminum signal and platelet morphology, indicating gibbsite, $Al(OH)_3$. The image captures

The pitted regions were examined at higher magnification to investigate the morphology of the redeposited aluminum-containing species. As shown Figure 11, the visible platelet morphology and the characteristic high elemental aluminum concentration are evidence of aluminum hydroxide $Al(OH)_3$ in the gibbsite form, which has a characteristic platelet structure and readily forms in acidic conditions when Al and OH are present [54–56].

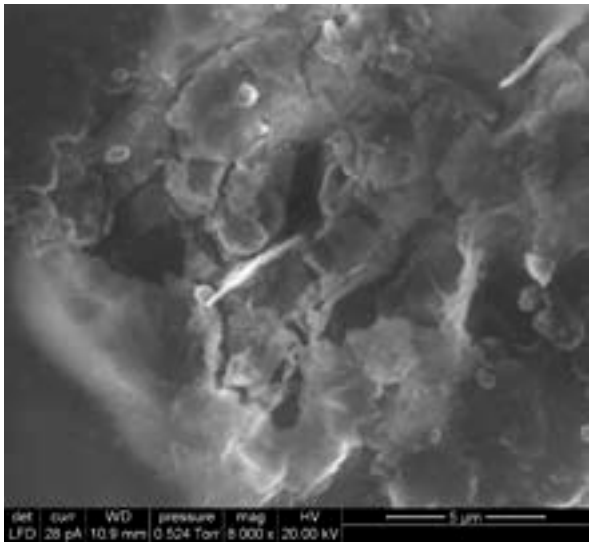

Figure 11. SEM micrograph, at 8000× magnification, of a pitted region of Istria stone treated with ALD alumina (S10_ALD) and immersed in acid solution. The area shown is in a pitted region with high aluminum signal and platelet morphology, indicating gibbsite, $Al(OH)_3$. The image captures secondary electrons.

4. Conclusions

In this work, atomic layer deposition has been explored as a method for applying protective amorphous alumina coatings to a compact carbonate stone (Istria stone). Istria stone is both representative of cultural heritage interests and representative of compact carbonate substrates in general. It was found that an advantage of such coatings, with respect to traditional polymeric protective treatments, is that the ALD alumina coatings do not significantly alter the surface morphology by filling open pores or accumulating on the surface in more compact areas. Additionally, the change in the appearance of the stone as measured by colorimetry is minimal, i.e., below generally accepted standards for cultural heritage interventions. We found that the protective effect of ALD alumina coatings was extremely promising, slowing the average rate of pH evolution and Ca^{2+} leaching dramatically when samples were subjected to aqueous acid immersion with an initial solution pH of 4. The eventual failure mechanisms of the ALD coatings during immersion were also investigated, with morphological findings suggesting that the failure mechanism involves the existence of small defect sites in the films, which lead to localized permeation, pitting, and finally redeposition in those areas but sustained protection in regions distant from such defects. Samples coated with the thickest films, formed by 500 cycles of ALD alumina, were most extensively studied in this work because they had the best protective effects against acid immersion. Because even these thickest coatings caused minimal appearance and morphological changes to the stone, the 500-cycle coatings are deemed most promising of those we have studied for application purposes. However, more in-depth analysis comparing the behavior of the different ALD coating thicknesses could provide more insight into the underlying kinetics of the ALD coatings as diffusion barriers and is the focus of future research. Further, our findings suggest new directions for future research in improving ALD coatings on stone, for example, by focusing on ways to eliminate the initial defects in the applied films. In addition, our future work will focus on improving the statistics related to ALD-coated stone's evolution in acid to better extrapolate more general trends and focus on other aspects relevant to cultural heritage applications, such as removability and direct comparison with current polymer treatments.

5. Patents

Patent disclosure in progress.

Supplementary Materials: The following supporting information can be downloaded at: https://www.mdpi.com/article/10.3390/coatings14080931/s1, Figure S1: Locations of the point spectra taken across various morphological features of an Istria stone sample coated with 500 cycles of ALD amorphous alumina; Figure S2: SEM-EDX point analysis results corresponding to locations in Figure S1. The Al wt% across the various features results in an average Al wt% of 7.2 ± 1.0. (**a**) Spectrum 7 (**b**) Spectrum 8 (**c**) Spectrum 9 (**d**) Spectrum 10.

Author Contributions: Conceptualization, G.P.B., E.B., E.Z. and R.J.P.; methodology, G.P.B., E.B., E.Z. and R.J.P.; validation, G.P.B., S.S., E.B., E.Z. and R.J.P.; formal analysis, G.P.B.; investigation, G.P.B. and S.S.; resources, G.P.B., S.S., E.B., E.Z. and R.J.P.; data curation, G.P.B.; writing—original draft preparation, G.P.B.; writing—review and editing, G.P.B., S.S., E.B., E.Z. and R.J.P.; visualization, G.P.B.; supervision, R.J.P., E.B. and E.Z.; project administration, G.P.B., E.B., E.Z. and R.J.P.; funding acquisition, G.P.B., R.J.P. and E.Z. All authors have read and agreed to the published version of the manuscript.

Funding: This collaboration was supported by an Open Study/Research grant awarded to G.P.B. from the Fulbright U.S. Student Program, sponsored by the U.S. Department of State and the Italy Fulbright Commission, awarded under the Authorization of the Mutual Educational and Cultural Exchange Act of 1961 (P.L.87.256) and under the terms of a diplomatic agreement between the Italian and United States Governments. The program is financed by both governments.

Institutional Review Board Statement: Not applicable.

Informed Consent Statement: Not applicable.

Data Availability Statement: The data are contained within the article.

Acknowledgments: We thankfully acknowledge the contributions to this work by John Abrams and the staff at the Nanofabrication Lab at the University of Maryland, Federico Zorzi at Centro di Analisi e Servizi Per la Certificazione at the University of Padua, and Laura Falchi and Alessandro Bonetto at Ca' Foscari University Venice.

Conflicts of Interest: The authors declare no conflicts of interest.

References

1. Brimblecombe, P. *The Effects of Air Pollution on the Built Environment*; Imperial College Press: London, UK, 2003; ISBN 978-1-84816-128-3.
2. Sabbioni, C. Mechanisms of Air Pollution Damage to Stone. In *Air Pollution Reviews*; Imperial College Press: London, UK, 2003; Volume 2, pp. 63–106. ISBN 978-1-86094-291-4.
3. Vidal, F.; Vicente, R.; Mendes Silva, J. Review of Environmental and Air Pollution Impacts on Built Heritage: 10 Questions on Corrosion and Soiling Effects for Urban Intervention. *J. Cult. Herit.* **2019**, *37*, 273–295. [CrossRef]
4. Vidović, K.; Hočevar, S.; Menart, E.; Drventić, I.; Grgić, I.; Kroflič, A. Impact of Air Pollution on Outdoor Cultural Heritage Objects and Decoding the Role of Particulate Matter: A Critical Review. *Environ. Sci. Pollut. Res.* **2022**, *29*, 46405–46437. [CrossRef] [PubMed]
5. Brimblecombe, P.; Grossi, C.M. Millennium-Long Damage to Building Materials in London. *Sci. Total Environ.* **2009**, *407*, 1354–1361. [CrossRef] [PubMed]
6. Ghedini, N.; Ozga, I.; Bonazza, A.; Dilillo, M.; Cachier, H.; Sabbioni, C. Atmospheric Aerosol Monitoring as a Strategy for the Preventive Conservation of Urban Monumental Heritage: The Florence Baptistery. *Atmos. Environ.* **2011**, *45*, 5979–5987. [CrossRef]
7. Belfiore, C.M.; Barca, D.; Bonazza, A.; Comite, V.; La Russa, M.F.; Pezzino, A.; Ruffolo, S.A.; Sabbioni, C. Application of Spectrometric Analysis to the Identification of Pollution Sources Causing Cultural Heritage Damage. *Environ. Sci. Pollut. Res.* **2013**, *20*, 8848–8859. [CrossRef] [PubMed]
8. Maas, R.; Grennfelt, P.; Amann, M.; Harnett, B.; Kerr, J.; Berton, E.; Pritula, D.; Reiss, I.; Almodovar, P.; Héroux, M.-E.; et al. *Towards Cleaner Air—Scientific Assessment Report 2016*; Narayana Press: Gylling, Denmark, 2016.
9. Grennfelt, P.; Engleryd, A.; Forsius, M.; Hov, Ø.; Rodhe, H.; Cowling, E. Acid Rain and Air Pollution: 50 Years of Progress in Environmental Science and Policy. *Ambio* **2020**, *49*, 849–864. [CrossRef] [PubMed]
10. Annual Mean NO2 Concentrations Observed at (Sub)Urban Background Stations. Available online: https://www.eea.europa.eu/data-and-maps/daviz/annual-mean-no2-concentration-observed-7#tab-googlechartid_chart_21 (accessed on 9 June 2024).
11. Trends in Atmospheric Concentrations of CO2 (Ppm), CH4 (Ppb) and N2O (Ppb), between 1800 and 2017. Available online: https://www.eea.europa.eu/data-and-maps/daviz/atmospheric-concentration-of-carbon-dioxide-5 (accessed on 9 June 2024).
12. Maravelaki-Kalaitzaki, P.; Biscontin, G. Origin, Characteristics and Morphology of Weathering Crusts on Istria Stone in Venice. *Atmos. Environ.* **1999**, *33*, 1699–1709. [CrossRef]

13. Biscontin, G.; Fassina, V.; Miaravelaki, P.; Zendri, E. Venice: Stone Material Behaviour in Connection with the Environment. *MRS Proc.* **1990**, *185*, 253. [CrossRef]
14. Gnemmi, M.; Falchi, L.; Zendri, E. Non-Invasive-Monitoring Methodology for the Evaluation of Environmental Impacts on Istrian Stone Surfaces in Venice. *Atmosphere* **2022**, *13*, 1036. [CrossRef]
15. Pivato, A.; Pegoraro, L.; Masiol, M.; Bortolazzo, E.; Bonato, T.; Formenton, G.; Cappai, G.; Beggio, G.; Giancristofaro, R.A. Long Time Series Analysis of Air Quality Data in the Veneto Region (Northern Italy) to Support Environmental Policies. *Atmos. Environ.* **2023**, *298*, 119610. [CrossRef]
16. Artesani, A.; Di Turo, F.; Zucchelli, M.; Traviglia, A. Recent Advances in Protective Coatings for Cultural Heritage–An Overview. *Coatings* **2020**, *10*, 217. [CrossRef]
17. Doehne, E.F.; Price, C.A. *Stone Conservation: An Overview of Current Research*, 2nd ed.; Research in Conservation; Getty Conservation Institute: Los Angeles, CA, USA, 2010; ISBN 978-1-60606-046-9.
18. Fistos, T.; Fierascu, I.; Doni, M.; Chican, I.E.; Fierascu, R.C. A Short Overview of Recent Developments in the Application of Polymeric Materials for the Conservation of Stone Cultural Heritage Elements. *Materials* **2022**, *15*, 6294. [CrossRef] [PubMed]
19. Melo, M.J.; Bracci, S.; Camaiti, M.; Chiantore, O.; Piacenti, F. Photodegradation of Acrylic Resins Used in the Conservation of Stone. *Polym. Degrad. Stab.* **1999**, *66*, 23–30. [CrossRef]
20. Gherardi, F.; Maravelaki, P.N. (Eds.) *Conserving Stone Heritage: Traditional and Innovative Materials and Techniques*; Cultural Heritage Science; Springer International Publishing: Cham, Swizerland, 2022; ISBN 978-3-030-82941-4.
21. Kim, H.-M.; Kim, D.-G.; Kim, Y.-S.; Kim, M.; Park, J.-S. Atomic Layer Deposition for Nanoscale Oxide Semiconductor Thin Film Transistors: Review and Outlook. *Int. J. Extrem. Manuf.* **2023**, *5*, 012006. [CrossRef]
22. Sheng, J.; Lee, J.-H.; Choi, W.-H.; Hong, T.; Kim, M.; Park, J.-S. Review Article: Atomic Layer Deposition for Oxide Semiconductor Thin Film Transistors: Advances in Research and Development. *J. Vac. Sci. Technol. A Vac. Surf. Film.* **2018**, *36*, 060801. [CrossRef]
23. George, S.M. Atomic Layer Deposition: An Overview. *Chem. Rev.* **2010**, *110*, 111–131. [CrossRef]
24. Ishibe, T.; Maeda, Y.; Terada, T.; Naruse, N.; Mera, Y.; Kobayashi, E.; Nakamura, Y. Resistive Switching Memory Performance in Oxide Hetero-Nanocrystals with Well-Controlled Interfaces. *Sci. Technol. Adv. Mater.* **2020**, *21*, 195–204. [CrossRef]
25. Rebenne, H.E.; Bhat, D.G. Review of CVD TiN Coatings for Wear-Resistant Applications: Deposition Processes, Properties and Performance. *Surf. Coat. Technol.* **1994**, *63*, 1–13. [CrossRef]
26. Kayanuma, M.; Choe, Y.-K.; Hagiwara, T.; Kameda, N.; Shimoi, Y. Theoretical Study of the Mechanism for the Reaction of Trimethylaluminum with Ozone. *ACS Omega* **2021**, *6*, 26282–26292. [CrossRef]
27. Oh, I.-K.; Sandoval, T.E.; Liu, T.-L.; Richey, N.E.; Nguyen, C.T.; Gu, B.; Lee, H.-B.-R.; Tonner-Zech, R.; Bent, S.F. Elucidating the Reaction Mechanism of Atomic Layer Deposition of $Al_2O_3$with a Series of $Al(CH_3)_xCl_{3-x}$ and $Al(C_yH_{2y+1})_3$ Precursors. *J. Am. Chem. Soc.* **2022**, *144*, 11757–11766. [CrossRef]
28. Puurunen, R.L.; Vandervorst, W. Island Growth as a Growth Mode in Atomic Layer Deposition: A Phenomenological Model. *J. Appl. Phys.* **2004**, *96*, 7686–7695. [CrossRef]
29. Naumann, V.; Otto, M.; Wehrspohn, R.B.; Werner, M.; Hagendorf, C. Interface and Material Characterization of Thin ALD-Al_2O_3 Layers on Crystalline Silicon. *Energy Procedia* **2012**, *27*, 312–318. [CrossRef]
30. Young, M.J.; Bedford, N.M.; Yanguas-Gil, A.; Letourneau, S.; Coile, M.; Mandia, D.J.; Aoun, B.; Cavanagh, A.S.; George, S.M.; Elam, J.W. Probing the Atomic-Scale Structure of Amorphous Aluminum Oxide Grown by Atomic Layer Deposition. *ACS Appl. Mater. Interfaces* **2020**, *12*, 22804–22814. [CrossRef] [PubMed]
31. Porter, D.A.; Easterling, K.E. *Phase Transformations in Metals and Alloys*, 2nd ed.; Springer-Science & Business Media: Berlin, Germany, 1992.
32. Ritala, M.; Leskelä, M.; Dekker, J.-P.; Mutsaers, C.; Soininen, P.J.; Skarp, J. Perfectly Conformal TiN and Al2O3 Films Deposited by Atomic Layer Deposition. *Chem. Vap. Depos.* **1999**, *5*, 7–9. [CrossRef]
33. Shkondin, E.; Takayama, O.; Lindhard, J.M.; Larsen, P.V.; Mar, M.D.; Jensen, F.; Lavrinenko, A.V. Fabrication of High Aspect Ratio TiO2 and Al2O3 Nanogratings by Atomic Layer Deposition. *J. Vac. Sci. Technol. A Vac. Surf. Film.* **2016**, *34*, 031605. [CrossRef]
34. Marquardt, A.E.; Breitung, E.M.; Drayman-Weisser, T.; Gates, G.; Phaneuf, R.J. Protecting Silver Cultural Heritage Objects with Atomic Layer Deposited Corrosion Barriers. *Herit. Sci.* **2015**, *3*, 37. [CrossRef]
35. Hiebert, M.E.; Weaver, J.; Lam, T.; Little, N.; Hyde, E.; Vicenzi, E.P.; Phaneuf, R.J.; Smithsonian Institution; National Institute of Standards and Technology. ALD Deposited Amorphous Alumina Coatings Can Slow Glass Alteration. *Phys. Chem. Glas. Eur. J. Glass Sci. Technol. B* **2022**, *63*, 97–110. [CrossRef]
36. Sundaram, G.M.; Bertuch, A.; Bhatia, R.; Coutu, R.; Dalberth, M.J.; Deguns, E.; Liu, G.; Sowa, M.J.; Becker, J.S. (Invited) Large Format Atomic Layer Deposition. *ECS Trans.* **2010**, *33*, 429–440. [CrossRef]
37. Beneq Launches the World's Largest ALD Reactor: The Beneq P1500. Available online: https://beneq.com/en/beneq-launches-the-worlds-largest-ald-reactor-the-beneq-p1500/ (accessed on 9 June 2024).
38. Puurunen, R.L. Surface Chemistry of Atomic Layer Deposition: A Case Study for the Trimethylaluminum/Water Process. *J. Appl. Phys.* **2005**, *97*, 121301. [CrossRef]
39. Groner, M.D.; Fabreguette, F.H.; Elam, J.W.; George, S.M. Low-Temperature Al_2O_3 Atomic Layer Deposition. *Chem. Mater.* **2004**, *16*, 639–645. [CrossRef]
40. Sciarretta, F.; Eslami, J.; Beaucour, A.-L.; Noumowé, A. State-of-the-Art of Construction Stones for Masonry Exposed to High Temperatures. *Constr. Build. Mater.* **2021**, *304*, 124536. [CrossRef]

41. Hutchinson, J.W. Stresses and Failure Modes in Thin Films and Multilayers: Notes for a Dcamm Course. 1996. Available online: https://citeseerx.ist.psu.edu/document?repid=rep1&type=pdf&doi=445a05fac9019c9be1f6ba77904e706f8ba262a3 (accessed on 9 June 2024).
42. Maravelaki-Kalaitzaki, P.; Bertoncello, R.; Biscontin, G. Evaluation of the Initial Weathering Rate of Istria Stone Exposed to Rain Action, in Venice, with X-Ray Photoelectron Spectroscopy. *J. Cult. Herit.* **2002**, *3*, 273–282. [CrossRef]
43. Costantini, R.; Balliana, E.; Dalla Torre, D.; Aricò, F.; Zendri, E. Evaluating the Impacts of Alcohol-Based Solutions on Silk: Chemical, Mechanical and Wettability Changes before and after Artificial Ageing. *Heritage* **2022**, *5*, 3588–3604. [CrossRef]
44. Izzo, F.C.; Balliana, E.; Perra, E.; Zendri, E. Accelerated Ageing Procedures to Assess the Stability of an Unconventional Acrylic-Wax Polymeric Emulsion for Contemporary Art. *Polymers* **2020**, *12*, 1925. [CrossRef] [PubMed]
45. Langereis, E.; Heil, S.B.S.; Knoops, H.C.M.; Keuning, W.; Van De Sanden, M.C.M.; Kessels, W.M.M. In Situ Spectroscopic Ellipsometry as a Versatile Tool for Studying Atomic Layer Deposition. *J. Phys. D Appl. Phys.* **2009**, *42*, 073001. [CrossRef]
46. Beche, E.; Fournel, F.; Larrey, V.; Rieutord, F.; Fillot, F. Direct Wafer Bonding of Amorphous or Densified Atomic Layer Deposited Alumina Thin Films. *Microsyst. Technol.* **2015**, *21*, 953–959. [CrossRef]
47. Chartier, G. *Introduction to Optics*; Advanced Texts in Physics; Springer: New York, NY, USA, 2005; ISBN 978-0-387-40346-5.
48. Johnston-Feller, R. Color Science in the Examination of Museum Objects: Nondestructive Procedures. *Color Res. Appl.* **2002**, *27*, 456–457. [CrossRef]
49. Sjöberg, E.L.; Rickard, D.T. Calcite Dissolution Kinetics: Surface Speciation and the Origin of the Variable pH Dependence. *Chem. Geol.* **1984**, *42*, 119–136. [CrossRef]
50. Ebert, W.L.; Bates, J.K. The Importance of Secondary Phases in Glass Corrosion. *MRS Proc.* **1990**, *212*, 89. [CrossRef]
51. Willis, S.A.; McGuinness, E.K.; Li, Y.; Losego, M.D. Re-Examination of the Aqueous Stability of Atomic Layer Deposited (ALD) Amorphous Alumina (Al_2O_3) Thin Films and the Use of a Postdeposition Air Plasma Anneal to Enhance Stability. *Langmuir* **2021**, *37*, 14509–14519. [CrossRef]
52. Parsons, R. Atlas of Electrochemical Equilibria in Aqueous Solutions. *J. Electroanal. Chem. Interfacial Electrochem.* **1967**, *13*, 471. [CrossRef]
53. Correa, G.C.; Bao, B.; Strandwitz, N.C. Chemical Stability of Titania and Alumina Thin Films Formed by Atomic Layer Deposition. *ACS Appl. Mater. Interfaces* **2015**, *7*, 14816–14821. [CrossRef] [PubMed]
54. Barnhisel, R.I.; Rich, C.I. Gibbsite, Bayerite, and Nordstrandite Formation as Affected by Anions, pH, and Mineral Surfaces. *Soil Sci. Soc. Am. J.* **1965**, *29*, 531–534. [CrossRef]
55. Schoen, R.; Roberson, C.E. Structures of Aluminum Hydroxide and Geochemical Implications. *Am. Mineral.* **1970**, *55*, 43–77.
56. Fan, W.; Li, W. Morphology-Control Techniques for Preparing Aluminum Hydroxide via Wet Chemical Synthesis. *Hydrometallurgy* **2020**, *192*, 105256. [CrossRef]